

# On Uplink CDMA Cell Capacity: Mutual Coupling and Scattering Effects on Beamforming

Alexander M. Wyglinski, *Student Member, IEEE*, and Steven D. Blostein, *Senior Member, IEEE*

**Abstract**—It has been shown that code-division multiple-access (CDMA) systems that employ digital beamforming and base-station antenna arrays have the potential to significantly increase capacity. Therefore, accurate performance prediction of such systems is important. We propose to take the electromagnetic behavior of the base-station antenna array into account, as well as its impact on wireless channel propagation. Specifically, the wide-band channel introduces scattering, while the mobile environment causes Doppler fading, which in turn degrades power controllability. We develop a more accurate performance analysis of antenna arrays, where the performance degradation in digital beamforming due to the combination of mutual coupling, scatter, and imperfect power control and its impact on uplink CDMA system capacity is quantified. In this analysis, a Rayleigh fading amplitude with varying angle-of-arrival spread is assumed, and maximum signal-to-noise ratio beamforming weights are used. These weights are further correlated with mutual coupling at the base-station array. Despite the degradation due to the combination of mutual coupling, scattering, and imperfect power control, significant capacity increases are possible.

**Index Terms**—Antenna arrays, code-division multiple access (CDMA), mutual coupling, power control, scatter, smart antennas.

## I. INTRODUCTION

ONE OF the significant challenges in enhancing the performance of next-generation communication systems involves making maximum use of limited spectrum while allowing for flexible multiple access. While code-division multiple access (CDMA) possesses a number of advantages for multiple access, its spectral efficiency is modest. Capacity analysis has been a subject of research for some time [1]. Recently, it has been proposed that greater frequency reuse can be achieved using multiple antenna arrays and digital beamforming at cellular base stations. In fact, this scenario has been analyzed previously, and significant uplink gains have been shown for both stream traffic capacity [2], [3] and Erlang capacity [4].

The objective of this paper is to investigate the performance of CDMA systems employing antenna arrays and digital beam-

forming under more realistic signal propagation assumptions. In particular, we develop a general method to analyze system performance taking into account mutual electromagnetic coupling of antenna array elements, scattering due to multipath propagation, and the effect of imperfectly power-controlled cell traffic. Rather than treat each of these effects separately, we demonstrate their combined interaction and effects on multiaccess interference (MAI) reduction.

Mutual coupling effects from an antenna array have been classically evaluated using an  $N$ -port network representation [5]–[8], where  $N$ -port circuit parameters form the elements of a mutual impedance matrix. For dipole antennas containing parallel thin elements, analytically tractable expressions can be obtained. To take into account finite metal thicknesses and more accurate current distributions, numerical techniques can be employed. Three methods for determining mutual impedances are employed and compared in this paper.

Recently, mutual coupling analysis has been extended to beam-pattern synthesis [9]. A simplified mutual coupling analysis [10] has been applied to determining the sensitivity of coherent binary phase-shift keying transmission using beamforming in fading channels with scatter [11]–[13]. The mutual coupling analysis of [12] and [13], in particular their expression for the mutual impedance they obtained from [10], is restricted to parallel side-by-side antennas of equal length and odd multiples of half the wavelength. The impact of antenna spacing, angle spread, and spatial correlation on single-user bit error rate performance was assessed.

The effects of scattering on plane wave propagation in antenna arrays may be conveniently quantified using a spatial dispersion parameter known as *angle spread* and applied to determining second-order multichannel statistics [14]–[17]. However, most of the techniques currently used for assessing the impact of scatter on CDMA system performance neglect the effects of mutual coupling in the base-station antenna array. Effects of scattering on signal amplitude and phase were considered separately and in the absence of mutual coupling [14]. In [2], it was shown that the interelement antenna cross-correlation matrix due to the combined effects of scattering and multiaccess interference can be approximated by white noise in certain propagation conditions. In [2], however, mutual coupling was ignored.

Typically, imperfect CDMA power-control performance is analyzed by modeling the target signal-to-noise ratio as a log-normally distributed random variable [1], [18]. This is partly due to the presence of scattering and its effects on the power levels received at the base station, thus influencing the CDMA system capacity. This effect has not previously been investigated

Manuscript received February 2, 2001; revised July 17, 2002. This paper was presented in part at the IEEE Vehicular Technology Conference (VTC-Fall 2000), Boston, MA, September 2000. This work was supported by the Canadian Institute for Telecommunications Research under the Networks of Centres of Excellence Program of the Government of Canada.

A. M. Wyglinski was with the Department of Electrical and Computer Engineering, Queen's University, Kingston, K7L 3N6 ON, Canada. He is now with the Department of Electrical and Computer Engineering, McGill University, Montréal, H3A 2A7 PQ, Canada (e-mail: alexw@tsp.ece.mcgill.ca).

S. D. Blostein is with the Department of Electrical and Computer Engineering, Queen's University, Kingston, K7L 3N6 ON, Canada (e-mail: sdb@ee.queensu.ca).

Digital Object Identifier 10.1109/TVT.2002.808797

in conjunction with mutual coupling effects. In this paper, we generalize the power-control analysis of [1] to the case of antenna arrays with mutual coupling and scattering.

Recently, the effects of mutual coupling on multiple-input multiple-output (MIMO) system capacity were assessed in [19]. By decreasing the amount of correlation between parallel channels, mutual coupling was shown to increase capacity. In this paper, we consider the special case of a single transmit antenna. In this single-channel case, MIMO capacity maximization reduces to that of signal-to-(noise plus interference) ratio (SINR) maximization. In the following, we assess the impact of digital beamforming on increasing system capacity through increasing uplink SINR.

This paper is organized as follows. Section II analyzes mutual coupling effects on beamforming through three alternative mutual impedance matrix calculations. Section III derives second-order multichannel statistics that combine the effects of mutual impedance and scattering due to multipath propagation. Section IV applies the new statistical model to uplink cell capacity estimation, while Section V extends capacity analysis to imperfect power control with combined scattering and mutual coupling effects. Numerical results are presented in Section VI.

## II. MUTUAL COUPLING EFFECTS

To model the effects of mutual coupling, we employ a mutual impedance matrix to characterize the interaction among antenna array components. We calculate elements of this matrix using the following three methods, in order of increasing accuracy and computational complexity: *induced electromotive force (EMF)*, the *method of moments*, and *full-wave electromagnetic numerical computation*. In each method, an  $N_A$ -element antenna array is represented as an  $N$ -port network. For induced EMF,  $N = N_A$ , while for the method of moments,  $N$  is an integer multiple of  $N_A$ , i.e., each antenna array is subdivided into equal-length increments, each corresponding to a port. Finally, in the case of full-wave electromagnetic numerical computation, the entire antenna, represented by a three-dimensional (3-D) computer-aided design model, is subdivided into  $N$  surface patches. In the following sections, we calculate the associated circuit parameters, i.e., the driving-point impedances, of each port. These impedances are organized into a mutual impedance matrix  $[Z]$  and then used in later sections for cell capacity prediction. In summary, the three methods each has a distinct approach to obtaining  $[Z]$ .

### A. Induced EMF

Induced EMF is a classical method of computing the self and mutual impedances of an  $N$ -port network representation of an antenna array [5], [6], [20]. Here, the Poynting vector, created from the electric and magnetic field, is integrated over the

array elements. This method is restricted to straight and parallel elements in formation and does not account for the radii of the wires and the gaps at the feeds. The advantage of induced EMF is that it leads to closed-form solutions, which provide for simple analysis. Following the approach of King [6], the elements of the mutual impedance matrix  $[Z]$ , can be shown as in (1) at the bottom of the page, where  $1 \leq m, n \leq N_A$  and where

$$\begin{aligned} R_{mn} = & 30 \cos(2\kappa l)(Ci(u_0) + Ci(v_0) - 2Ci(u_1) \\ & - 2Ci(v_1) + 2Ci(\kappa d)) + 30 \sin(2\kappa l)(-Si(u_0) \\ & + Si(v_0) + 2Si(u_1) - 2Si(v_1)) \\ & + 30(-2Ci(u_1) - 2Ci(v_1) + 4Ci(\kappa d)) \end{aligned}$$

$$\begin{aligned} X_{mn} = & 30 \cos(2\kappa l)(-Si(u_0) - Si(v_0) + 2Si(u_1) \\ & + 2Si(v_1) - 2Si(\kappa d)) + 30 \sin(2\kappa l)(-Ci(u_0) \\ & + Ci(v_0) + 2Ci(u_1) - 2Ci(v_1)) \\ & + 30(2Si(u_1) + 2Si(v_1) - 4Si(\kappa d)) \end{aligned}$$

$$u_0 = \kappa(\sqrt{d^2 + 4l^2} - 2l) \quad v_0 = \kappa(\sqrt{d^2 + 4l^2} + 2l)$$

$$u_1 = \kappa(\sqrt{d^2 + l^2} - l) \quad v_1 = \kappa(\sqrt{d^2 + l^2} + l)$$

$$Ci(u) = \int_{\infty}^u \frac{\cos(x)}{x} dx \quad Si(u) = \int_0^u \frac{\sin(x)}{x} dx.$$

$d$  is the horizontal distance between dipole antennas  $m$  and  $n$ ,  $l$  is half the length of the dipole antenna, and  $\kappa = 2\pi/\lambda$  is the wave number. Since the above expression only depends on interelement distances, arbitrary arrangements of array elements can be considered. The matrix  $[Z]$  can account for mutual coupling within beam-pattern synthesis by solving for the output current via the matrix equation  $[Z]^{-1} \vec{V} = \vec{I}$ , where  $\vec{V}$  and  $\vec{I}$  are, respectively, the vectors of the voltages and currents along each antenna and  $[Z]^{-1}$  is the matrix inverse of  $[Z]$ . Given an ideal voltage beampattern  $\vec{V}$ , the output beampattern for  $N_A$  antenna elements is given by

$$A(\theta) = \left| \sum_{m=1}^{N_A} I_m \beta_m e^{j\alpha_m} \right|^2 \quad (2)$$

where  $I_m$  is the  $m$ th element of  $\vec{I}$  and  $\theta$  is the desired angle of arrival (AOA) for the beampattern.

To illustrate the effects of mutual coupling, let us refer to the two sample beampatterns from a four-element circular array using  $\lambda/2$ -dipole antennas shown in Fig. 1. The horizontal separation distance  $d$  between two adjacent antennas in the array is equal to  $\lambda/2 = 75$  mm, while for two opposite antennas, it is

$$Z_{mn} = \begin{cases} 30(0.5772 + \ln(2\kappa l) - Ci(2\kappa l)) + j30(Si(2\kappa l)), & m = n \\ R_{mn} + jX_{mn}, & m \neq n \end{cases} \quad (1)$$

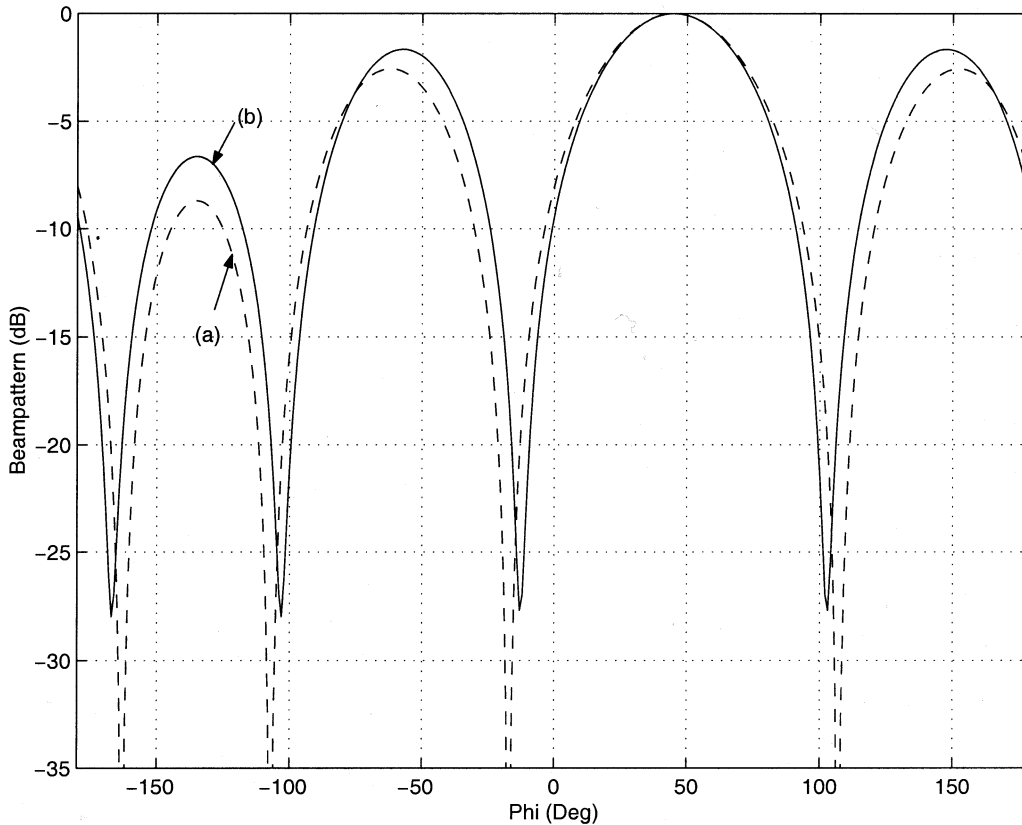


Fig. 1. Beampattern of a four-element circular array with AOA= 45°. (a) No mutual coupling effects and (b) induced EMF method-generated mutual coupling effects.

$\lambda/\sqrt{2} = 106.1$  mm. Furthermore, we are using  $\beta_m = 1$ , for all  $m$ , and

$$\alpha_m = \frac{\pi \cos\left(\theta - m\left(\frac{2\pi}{N_A}\right)\right)}{2 \sin\left(\frac{\pi}{N_A}\right)} \quad (3)$$

in (2). Finally, referring to Fig. 1, beampattern (b) includes the effects of mutual coupling, generated using the induced EMF method, while beampattern (a) does not. By observing these beampatterns, it can be stated that the mutual coupling effects can cause higher sidelobe levels and a broader main lobe.

### B. Method of Moments

For greater accuracy, we may partition each antenna of the array into equal-length segments and apply the method of moments [7], [8]. We have found that using 15 segments per element gives a reasonable tradeoff between accuracy and complexity. Using electromagnetic theory and assuming unidirectional current flow, the current and charge densities are approximated by viewing the antenna array as filaments of current and charge on the wire axis. Using the method in [7], an expression for mutual impedance matrix elements  $1 \leq m, n \leq N$  is shown to be

$$Z_{mn} = j\omega\mu\Delta\vec{l}_n \cdot \Delta\vec{l}_m\psi(n, m) + \frac{1}{j\omega\epsilon}[\psi(n^+, m^+) - \psi(n^-, m^+) - \psi(n^+, m^-) + \psi(n^-, m^-)] \quad (4)$$

$$\psi(n, m) = \frac{1}{\Delta l_n} \int_{\Delta l_n} \frac{e^{-jkR_m}}{4\pi R_m} dl \quad (5)$$

$$R_m = \begin{cases} \sqrt{\rho^2 + (z - z_m)^2}, & m \neq n \\ \sqrt{a^2 + z^2}, & m = n \end{cases} \quad (6)$$

where  $\rho$  is the horizontal distance between antennas containing points  $n$  and  $m$ ,  $a$  is the dipole antenna radius,  $k$  is the wave number,  $z_m$  is the vertical distance between points  $n$  and  $m$ ,  $\mu$  is the permeability,  $\epsilon$  is the permittivity,  $\Delta l_n$  is the length of the  $n^{\text{th}}$  increment,  $\omega$  is the frequency of operation (in radians per second), and  $n^-$  and  $n^+$  denote the starting and terminating points of the  $n^{\text{th}}$  increment, respectively.

To perform beampattern synthesis, numerical integration of (5) is required. Again we obtain  $\vec{I} = [Z]^{-1}\vec{V}$ , where  $\vec{V}$  now specifies a vector of the incremental voltages and  $\vec{I}$  specifies a vector of the incremental currents. If the antennas are center-fed, only the increments corresponding to the centers of the antennas will have a nonzero voltage. Upon obtaining  $\vec{I}$ , we perform beampattern synthesis by determining the far-zone field at a point  $i$  using [8]

$$A_i = \frac{\mu e^{-jkr_i}}{4\pi r_i} \sum_{j=1}^n I_j e^{jkr_j \cos \xi_{ij}} \Delta l_j \quad (7)$$

where  $r_i$  and  $r_j$  are the radius vectors to the distant field and source points, respectively, and  $\xi_{ij}$  is the angle between them.

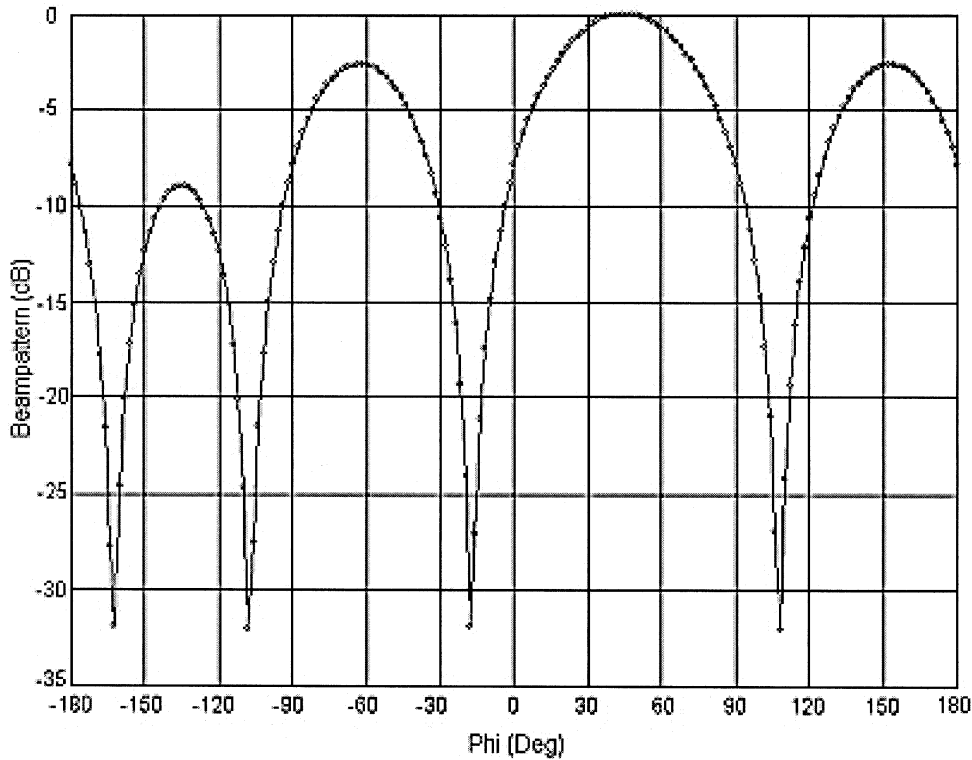


Fig. 2. Beam pattern of a four-element circular array with AOA= 45° and 3-D full-wave-generated mutual coupling effects.

The beam pattern corresponding to the four-element circular array mentioned earlier reveals a pattern nearly identical to that obtained by the induced EMF method in Fig. 1.

### C. Full-Wave Electromagnetic Numerical Computation

Full-wave electromagnetic numerical computation models both the electric current on a metallic structure and a magnetic current representing the field distribution on a metallic aperture. In this approach, we solve an integral equation derived using Green's functions and the method of moments. An element of the mutual impedance matrix  $[Z]$ ,  $Z_{mn}$ , is given as [21]

$$Z_{mn} = \int_S \{Z_s \vec{B}_m \cdot \vec{B}_n\} ds + \int_S ds \int_{S'} \{ \vec{B}_m \cdot \vec{G}(\vec{r}|\vec{r}') \cdot \vec{B}_n \} ds' \quad (8)$$

where  $Z_s$  is the surface impedance of the antenna increment with surface  $S$ ,  $\vec{B}_n(\vec{r})$  is a basis function, and  $\vec{G}(\vec{r}|\vec{r}')$  is Green's function. In our analysis, we chose a typical value of 40 increments per wavelength. To perform beam pattern synthesis, the voltage vector is determined from an incident electric field  $E_i$  by evaluating

$$V_n = \int_S \{ \vec{E}_i(\vec{r}) \cdot \vec{B}_n \} ds \quad (9)$$

and using (8), we again solve for  $\vec{T}$ . It should be noted that the differences among full-wave electromagnetic numerical computation formulations are based on the choice of basis functions  $\vec{B}_n(\vec{r})$  for the current distribution representation and Green's functions  $\vec{G}(\vec{r}|\vec{r}')$ .

A sample beam pattern, generated using the IE3D software package [21], is shown in Fig. 2. This beam pattern is generated using the same four-element circular array setup used to create the beam patterns in Fig. 1. Moreover, the antennas designed with this software have a radius of 0.075 mm and a conductivity of  $4.9 \times 10^7$  U/m. The operating environment is an air-filled region with no ground plane. Therefore, observing Fig. 2, the beam pattern has a broadened main beamwidth and increased sidelobe levels when compared to beam pattern (a) in Fig. 1, and it is similar to beam pattern (b).

### III. SCATTERING EFFECTS

Scatter is a phenomenon associated with multipath propagation, occurring when signals from a single source arrive at a base station from several directions within an angular region after being reflected by objects in the surrounding environment. This angular region, known as the *angle spread*, varies according to the operating environment, from a few degrees in flat rural areas to 360° in indoor picocell environments [20], [22].

In this section, the derivation of the cross-correlation statistics for a multipath fading channel is generalized to include mutual coupling effects. With these statistics, system cell capacity incorporating scatter as well as mutual coupling can be determined.

Note that throughout the remainder of this paper, the mutual coupling effects used in the analysis will be modeled using the analytically tractable induced EMF method rather than the other two methods, without any appreciable loss in accuracy. This choice is due to the similar beam patterns of Figs. 1 and 2 as well as their similar capacity results [20].

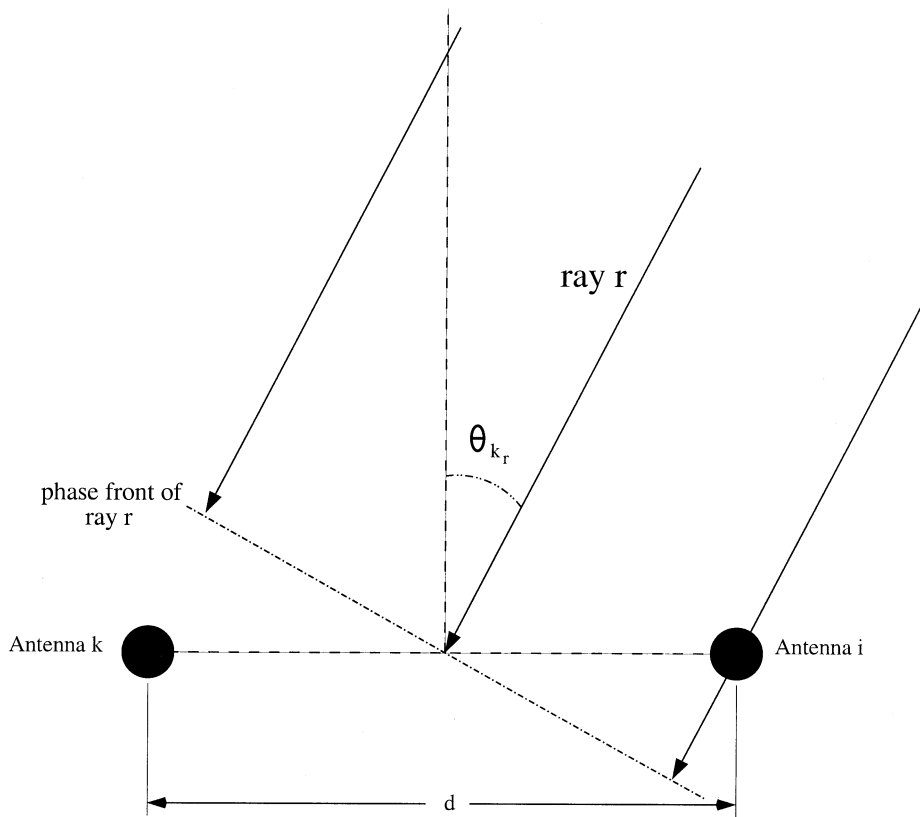


Fig. 3. Model used in our cross-correlation derivation.

### A. Cross-Correlation Statistics

Derivations of spatiotemporal cross-correlation statistics of the multipath fading channel may be found in [12]–[15], [17], and [22]. In particular, [12] and [13] extend these derivations to include the effects of mutual coupling as well as employed Nakagami- $m$  distributions to model the fading statistics of the channel. Nevertheless, the derivation in [12] and [13] is restricted to a specific azimuthal angle-of-arrival distribution. Moreover, the expressions for the mutual impedance used in [12] and [13] are only applicable to a specific array configuration and antenna length. In the following, such restrictions are removed in our derivation of the cross-correlation statistics where the effects of mutual coupling have been included.

Assume that we have two identical antennas denoted as  $i$  and  $k$  that are spaced a distance  $d$  apart receiving signals from the same source. Let the direction of the  $r^{\text{th}}$  wave form an angle  $\theta_{ik_r}$  with respect to a line passing through the two antennas. Suppose the  $r^{\text{th}}$  wave produces the voltages

$$v_{i_r} = a_r \cos \left( \omega t + \psi_r + \frac{\pi d}{\lambda} \cos(\theta_{ik_r}) \right) \quad (10)$$

$$v_{k_r} = a_r \cos \left( \omega t + \psi_r - \frac{\pi d}{\lambda} \cos(\theta_{ik_r}) \right) \quad (11)$$

on antennas  $i$  and  $k$ , respectively, for a coplanar wave of angular frequency  $\omega$  and wavelength  $\lambda$ . The phase delay of the ray  $r$  is represented by  $\psi_r$ , while the amplitude of the ray  $r$  is defined as  $a_r$  (see Fig. 3).

By the principle of superposition, the total voltage produced by a total of  $n$  plane waves at antennas  $i$  and  $k$  is given, respectively, by

$$v_i = \sum_{r=1}^n a_r \cos \left( \omega t + \psi_r + \frac{\pi d}{\lambda} \cos(\theta_{k_r}) \right) \quad (12)$$

$$\equiv A_i \cos(\omega t + \Psi_i)$$

$$v_k = \sum_{r=1}^n a_r \cos \left( \omega t + \psi_r - \frac{\pi d}{\lambda} \cos(\theta_{k_r}) \right) \quad (13)$$

$$\equiv A_k \cos(\omega t + \Psi_k)$$

such that the amplitudes  $a_r$  and phases  $\psi_r$  of each of the  $n$  wavefronts are distinct.

In (12) and (13), it can be easily shown that the mean signal voltages at antennas  $i$  and  $k$  are zero. Their mean-square signal voltages are

$$\overline{v_i^2} = \overline{v_k^2} = \frac{1}{2} \sum_{r=1}^n a_r^2 \quad (14)$$

where  $\overline{(\cdot)}$  denotes expectation. Assuming that  $A_i$ ,  $A_k$ ,  $\Psi_i$ , and  $\Psi_k$  are mutually independent, the mean-square signal amplitude at antennas  $i$  and  $k$  is

$$\overline{A_i^2} = \overline{A_k^2} = 2\overline{v_i^2}. \quad (15)$$

For a continuous probability distribution of waves, the above summation becomes an integral over a distribution  $f(\theta)$ , i.e.,

$$\overline{v_i^2} = \overline{v_k^2} = \int_0^{2\pi} f(\theta) d\theta. \quad (16)$$

To include the effects of mutual coupling, define a mutual admittance matrix  $[Y] = [Z]^{-1}$ . Without loss of generality, we will consider  $[Z]$  to be  $N_A$ -dimensional, corresponding to the induced EMF method. A pair of antennas  $i$  and  $k$  then have voltages  $v_{i,mc}$  and  $v_{k,mc}$ , where

$$\begin{aligned} \begin{bmatrix} v_{i,mc} \\ v_{k,mc} \end{bmatrix} &= \begin{bmatrix} |Y_{ii}| e^{j\angle Y_{ii}} & |Y_{ik}| e^{j\angle Y_{ik}} \\ |Y_{ki}| e^{j\angle Y_{ki}} & |Y_{kk}| e^{j\angle Y_{kk}} \end{bmatrix} \begin{bmatrix} v_i \\ v_k \end{bmatrix} \\ &\equiv \begin{bmatrix} B_{ic} \cos \omega t + B_{is} \sin \omega t \\ B_{kc} \cos \omega t + B_{ks} \sin \omega t \end{bmatrix} \end{aligned} \quad (17)$$

where, for example,  $|Y_{ik}|$  and  $\angle Y_{ik}$  represent the magnitude and phase of the mutual admittance between antenna elements  $i$  and  $k$ , respectively.

Since the phase angles  $\psi_r$  are assumed to be random and the number of scattered waves  $n$  is assumed to be large, the central limit theorem may be invoked and  $B_{ic}$ ,  $B_{is}$ ,  $B_{kc}$ , and  $B_{ks}$  are distributed normally with zero mean.

To determine the joint probability distribution of  $A_i$  and  $A_k$ , the second moments  $\overline{B_{ic}^2}$ ,  $\overline{B_{is}^2}$ ,  $\overline{B_{kc}^2}$ ,  $\overline{B_{ks}^2}$ ,  $\overline{B_{ic}B_{kc}^*}$ ,  $\overline{B_{is}B_{ks}^*}$ ,  $\overline{B_{ic}B_{is}^*}$ ,  $\overline{B_{kc}B_{ks}^*}$ ,  $\overline{B_{ic}B_{ks}^*}$ , and  $\overline{B_{kc}B_{is}^*}$  must be obtained. Fortunately, we can simplify the resulting expressions using the fact that the mutual admittance matrix is symmetric with equal elements along its diagonal. After some tedious algebra (see the Appendix), we obtain

$$\begin{aligned} \overline{B_{ic}^2} &= \overline{B_{is}^2} = \overline{B_{kc}^2} = \overline{B_{ks}^2} \\ &= \left( |Y_{ii}|^2 + |Y_{ik}|^2 \right) \frac{1}{2} \sum_{r=1}^m a_r^2 \\ &\quad + |Y_{ii}| |Y_{ik}| \sum_{r=1}^m a_r^2 \cos \left( \frac{2\pi d}{\lambda} \cos(\theta_{ik_r}) \right) \\ &\quad \cdot \cos(\angle Y_{ii} - \angle Y_{ik}) \\ &\equiv \rho_o \end{aligned} \quad (18)$$

$$\begin{aligned} \overline{B_{ic}B_{is}} &= \overline{B_{kc}B_{ks}} = 0 \\ \overline{B_{ic}B_{kc}} &= \overline{B_{is}B_{ks}} \end{aligned} \quad (19)$$

$$\begin{aligned} &= |Y_{ii}| |Y_{ki}| \sum_{r=1}^m a_r^2 \cos(\angle Y_{ii} - \angle Y_{ki}) \\ &\quad + \left( |Y_{ii}|^2 + |Y_{ik}|^2 \right) \\ &\quad \cdot \frac{1}{2} \sum_{r=1}^m a_r^2 \cos \left( \frac{2\pi d}{\lambda} \cos(\theta_{k_r}) \right) \\ &\equiv \rho_{R_i R_k} \end{aligned} \quad (20)$$

$$\begin{aligned} \overline{B_{ic}B_{ks}} &= -\overline{B_{kc}B_{is}} \\ &= - \left( |Y_{ii}|^2 - |Y_{ik}|^2 \right) \\ &\quad \cdot \frac{1}{2} \sum_{r=1}^m a_r^2 \sin \left( \frac{2\pi d}{\lambda} \cos(\theta_{k_r}) \right) \\ &\equiv \rho_{R_i I_k} \end{aligned} \quad (21)$$

where  $\rho_{R_i R_k}$  and  $\rho_{R_i I_k}$  are the cross-correlation coefficients of the real component of the Rayleigh fading value at antenna element  $i$  with the real and imaginary components of the Rayleigh fading value at antenna element  $k$ , respectively, and  $\rho_o$  is the mean-squared value of  $B_{ic}$ ,  $B_{is}$ ,  $B_{kc}$  and  $B_{ks}$ .

Applying (16) to (20) and (21), we finally obtain

$$\begin{aligned} \rho_{R_i R_k} &= 2|Y_{ii}| |Y_{ki}| \int_0^{2\pi} f(\theta) \cos(\angle Y_{ii} - \angle Y_{ki}) d\theta \\ &\quad + \left( |Y_{ii}|^2 + |Y_{ik}|^2 \right) \\ &\quad \cdot \int_0^{2\pi} f(\theta) \cos \left( \frac{2\pi d}{\lambda} \cos(\theta) \right) d\theta \end{aligned} \quad (22)$$

$$\begin{aligned} \rho_{R_i I_k} &= - \left( |Y_{ii}|^2 - |Y_{ik}|^2 \right) \\ &\quad \cdot \int_0^{2\pi} f(\theta) \sin \left( \frac{2\pi d}{\lambda} \cos(\theta) \right) d\theta. \end{aligned} \quad (23)$$

To determine (22) and (23), we need to specify  $f(\theta)$ , the probability density function (pdf) of the azimuth. This pdf depends on the spatial channel model and is typically either Gaussian or Laplacian distributed [23], [24]. In the next section, we employ a Gaussian angle of the arrival channel model that corresponds to a single cluster of scatterers as encountered in a narrow-band channel. This model has been verified by measurements [25]–[27]. The narrow-band channel is consistent with the unresolvable multipath fading model considered in this paper. We note that for the case of wider band CDMA with significant multipath delay spread, a Laplacian model tends to more closely fit experimental data [28].

#### B. Example: Gaussian Angle-of-Arrival Spatial Distribution

For a Gaussian angle-of-arrival (GAA) spatial channel model [24], we have a Gaussian distributed  $f(\theta)$  with mean angle-of-arrival  $\theta_k$  and variance  $\sigma_\Delta^2$ , namely

$$f(\theta) = \frac{1}{\sqrt{2\pi\sigma_\Delta^2}} e^{-(\theta-\theta_k)^2/2\sigma_\Delta^2}. \quad (24)$$

Substitution into (22) and (23), after some manipulation, yields the following approximations:

$$\begin{aligned} \rho_{R_i R_k} &\approx 2|Y_{ii}| |Y_{ki}| \cos(\angle Y_{ii} - \angle Y_{ki}) \\ &\quad \cdot \left( \operatorname{erf} \left( \frac{2\pi - \theta_k}{\sigma_\Delta} \right) + \operatorname{erf} \left( \frac{\theta_k}{\sigma_\Delta} \right) \right) \\ &\quad + \left( |Y_{ii}|^2 + |Y_{ik}|^2 \right) \\ &\quad \cdot \left( J_0 \left( \frac{2\pi d}{\lambda} \right) \right. \\ &\quad \left. + 2 \sum_{m=1}^{\infty} J_{2m} \left( \frac{2\pi d}{\lambda} \right) \cos(2m\theta_k) e^{-2m^2\sigma_\Delta^2} \right) \end{aligned} \quad (25)$$

$$\begin{aligned} \rho_{R_i I_k} &\approx - \left( |Y_{ii}|^2 - |Y_{ik}|^2 \right) \\ &\quad \cdot \left( 2 \sum_{m=1}^{\infty} J_{2m+1} \left( \frac{2\pi d}{\lambda} \right) \right. \\ &\quad \left. \cdot \sin((2m+1)\theta_k) e^{-(2m+1)^2\sigma_\Delta^2/2} \right) \end{aligned} \quad (26)$$

where  $J_{2m}(\cdot)$  denotes the Bessel function of the first kind of order  $2m$  and error function

$$\operatorname{erf}(x) \equiv \frac{2}{\sqrt{\pi}} \int_0^x e^{-t^2/2} dt.$$

In determining (25) and (26), the integrals are taken over  $[0, 2\pi)$  radians. The approximations arise from the Gaussian AOA distribution's being truncated to lie within the  $[0, 2\pi)$  range. As the angle spread  $\sigma_\Delta^2$  increases, this truncation effect is more pronounced.

#### IV. CDMA CELL CAPACITY ESTIMATION

In this section, we extend the CDMA results in [29] to the case of a perfectly power-controlled single-cell with a base-station array consisting of  $N_A$  antennas, taking into account the effects of mutual coupling and scattering [30]. In Section V, we will extend these results to imperfect power control.

Suppose first that  $N_A = 1$  and we denote the received signal power from  $N_M$  mobiles by  $P_R$ . Assume without loss of generality that the voice activity factor  $\alpha$  is unity with data transmission at rate  $R_B$  bits/s. The signal-to-noise ratio (SNR) is given as [29]

$$\text{SNR} = \frac{P_R}{(N_M - 1)P_R + \eta} \quad (27)$$

where  $\eta$  is the background noise power due to spurious interference and thermal noise within the bandwidth  $B$  of the spread signal. Using (27), the bit energy-to-noise density ratio is [29]

$$\frac{E_b}{N_o} = \frac{\frac{P_R}{R_B}}{(N_M - 1)\frac{P_R}{B} + \sigma_n^2} \quad (28)$$

where  $\sigma_n^2 \equiv \eta/B$  is the variance of the zero-mean in-band background noise.

In the multiple antenna element case ( $N_A > 1$ ) with beamforming, we generalize (28) to

$$\frac{E_b}{N_o} = \frac{E\{\tilde{P}_D\} \frac{P_R}{R_B}}{E\{\tilde{P}_I\} P_R \frac{(N_M - 1)}{B} + N_A \sigma_n^2} \quad (29)$$

where  $E\{\tilde{P}_D\}$  and  $E\{\tilde{P}_I\}$  denote the expected fraction of the desired mobile's power and interference, respectively, at the output of the beamformer. In (29), we assume that independent and identically distributed background noise is received at each antenna, which accounts for the  $N_A \sigma_n^2$  term in the denominator of (29) [3], [14], [31], [23]. In [31], it is shown that the second term in the denominator of (29) can be neglected without any significant loss in accuracy, and thus we may approximate the system capacity via

$$N_M = \left\lfloor \frac{1}{E\{\tilde{P}_I\}} \frac{E\{\tilde{P}_D\} B}{R \left(\frac{E_b}{N_o}\right)} \right\rfloor + 1 \quad (30)$$

where  $\lfloor \cdot \rfloor$  is the floor function.

##### A. Determining $E\{\tilde{P}_I\}$ and $E\{\tilde{P}_D\}$

We now determine the key parameters that capture the effects of beamforming—the expected interference  $E\{\tilde{P}_I\}$  and the expected mobile power  $E\{\tilde{P}_D\}$ —while taking into account the effects of mutual coupling and scattering. Without loss of generality, the following discussion is consistent with matrix di-

mensions corresponding to the induced EMF method. The discussion also pertains to the other methods of mutual impedance calculation after suitable zero padding and/or repetition of the voltage and current vector elements.

To account for the effects of mutual coupling, if a voltage beamforming vector  $\vec{\omega}(\theta_d)$  is applied to the received signals, the resulting current vector is [32]

$$\vec{\omega}_{MC}(\theta_d) \equiv [Z]^{-1} \vec{\omega}(\theta_d) = [Y] \vec{\omega}(\theta_d) \quad (31)$$

where  $[Y] = [Z]^{-1}$  is the  $N_A$  by  $N_A$  mutual admittance matrix and  $\theta_d$  is the AOA for the desired user. Throughout this paper, we have chosen  $\vec{\omega}(\theta_D)$  to be an ideal maximum SNR beamforming weight vector. Although the true array response vector would not be known in practice, this type of beamforming is useful for providing an upper bound on achievable system capacity for a single-user receiver.

Denote the  $N_A \times N_A$  received signal strength matrix  $[\beta]_k$  at mobile  $k$  as

$$[\beta]_k = \begin{bmatrix} \beta_{k1} & 0 & \cdots & 0 \\ 0 & \beta_{k2} & & \vdots \\ \vdots & & \ddots & 0 \\ 0 & \cdots & 0 & \beta_{kN_A} \end{bmatrix}. \quad (32)$$

We define the array response vector as

$$\vec{a}_\beta(\theta_k) \equiv \begin{bmatrix} \beta_{k1} \\ \beta_{k2} e^{j\alpha_1(\theta_k)} \\ \vdots \\ \beta_{kN_A} e^{j\alpha_{(N_A-1)}(\theta_k)} \end{bmatrix} \quad (33)$$

where  $\alpha_i$  is the phase at the  $i$ th element. For the case of a circular array and AOA  $\theta_d$ ,  $\alpha_i(\theta_d)$  is given by (3).

Using (31) and (33), define the normalized interference power due to an interferer  $k$  at angle-of-arrival  $\theta_k$  as

$$\phi_k(\theta_d, \theta_k) \equiv \left| \frac{\vec{\omega}_{MC}^{\mathbf{H}}(\theta_d) \vec{a}_\beta(\theta_k)}{\|\vec{\omega}_{MC}^{\mathbf{H}}(\theta_d)\| \|\vec{a}_\beta(\theta_k)\|} \right|^2 \quad (34)$$

where  $\vec{\omega}_{MC}^{\mathbf{H}}(\theta_d)$  denotes the complex conjugate transpose of  $\vec{\omega}_{MC}(\theta_d)$  and  $\|\cdot\|$  is the Euclidean norm over the complex plane.

The numerator in (34), after substituting the three previous equations, becomes

$$\begin{aligned} & \left| \vec{\omega}_{MC}^{\mathbf{H}}(\theta_d) \vec{a}_\beta(\theta_k) \right|^2 \\ &= \left| ([Y] \vec{\omega}(\theta_d))^{\mathbf{H}} ([\beta]_k \vec{a}(\theta_k)) \right|^2 \\ &= \left| \vec{\omega}^{\mathbf{H}}(\theta_d) [Y]^{\mathbf{H}} [\beta]_k \vec{a}(\theta_k) \right|^2 \\ &= \vec{\omega}^{\mathbf{H}}(\theta_d) [Y]^{\mathbf{H}} [\beta]_k \vec{a}(\theta_k) \vec{a}^{\mathbf{H}}(\theta_k) [\beta]_k^{\mathbf{H}} [Y] \vec{\omega}(\theta_d) \\ &= \sum_{i=1}^{N_A} \sum_{l=1}^{N_A} \sum_{p=1}^{N_A} \sum_{r=1}^{N_A} \beta_{ki} \beta_{kr}^* Y_{li}^* Y_{rp} \Theta_{ilpr} \end{aligned} \quad (35)$$

where

$$\Theta_{ilpr} = e^{j(\alpha_i(\theta_k) + \alpha_p(\theta_d) - \alpha_r(\theta_k) - \alpha_l(\theta_d))} \quad (36)$$

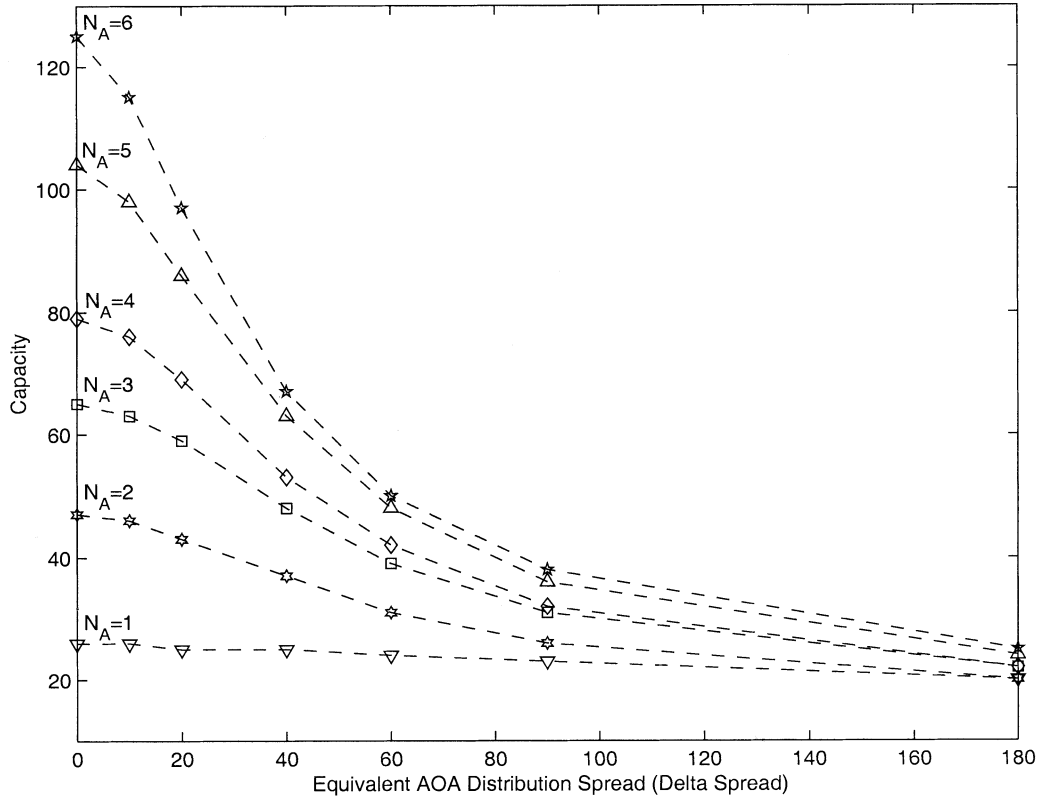


Fig. 4. System capacity predictions for a Gaussian angle-of-arrival distribution with no mutual coupling.

and  $\alpha_i(\theta_k)$ ,  $\alpha_l(\theta_d)$ ,  $\alpha_p(\theta_k)$ , and  $\alpha_r(\theta_d)$  are the phases of the array elements and  $Y_{li}$  and  $Y_{rp}$  are elements of  $[Y]$ .

The denominator terms of (34) can be expressed, respectively, as

$$\begin{aligned} \|\vec{a}_\beta(\theta_k)\| &= \left( ([\beta]_k \vec{a}(\theta_k))^H ([\beta]_k \vec{a}(\theta_k)) \right)^{1/2} \\ &= ([\beta]_k^H [\beta]_k)^{1/2} \\ &= \sum_{i=1}^{N_A} \beta_{ki}^2 \quad (37) \\ \|\vec{w}_{MC}^H(\theta_d)\| &= \left( (\vec{w}_{MC}^H(\theta_d))^H (\vec{w}_{MC}^H(\theta_d)) \right)^{1/2} \\ &= ([Y] \vec{w}(\theta_d) \vec{w}^H(\theta_d) [Y]^H)^{1/2} \\ &= \sum_{h=1}^{N_A} \sum_{s=1}^{N_A} \sum_{m=1}^{N_A} e^{j(\alpha_h(\theta_d) - \alpha_s(\theta_d))} Y_{sm}^* Y_{mh}. \quad (38) \end{aligned}$$

The amplitude term can be factored as  $\beta_{ki} = \eta_k R_{ki}$ , where  $\eta_k$  is a path loss plus shadowing factor at mobile  $k$ , and  $R_{ki}$  is the Rayleigh fading random variable for mobile  $k$  at the  $i$ th array element. Both  $\eta_k$  and  $R_{ki}$  are mutually independent, and each is a function of two Gaussian distributed random variables. The shadowing factor  $\eta_k$  is assumed to be identically distributed across the antenna array.

Since both  $\theta_k$  and  $\theta_d$  are assumed to be random variables uniformly distributed over  $[0, 2\pi)$ , it can be shown that after

substitution of  $\beta_{ki} = \eta_k R_{ki}$  into the expected values of (35) and (37) conditioned on  $\theta_k$ ,  $\theta_d$  and  $\sigma_\Delta^2$  are, respectively

$$\begin{aligned} E \left\{ \sum_{i=1}^{N_A} \sum_{l=1}^{N_A} \sum_{p=1}^{N_A} \sum_{r=1}^{N_A} \eta_k^2 R_{ki} R_{kr} Y_{li}^* Y_{rp} \Theta_{ilpr} \middle| \theta_k, \theta_d, \sigma_\Delta^2 \right\} \\ = E \{ \eta_k^2 \} \sum_{i=1}^{N_A} \sum_{l=1}^{N_A} \sum_{p=1}^{N_A} \sum_{r=1}^{N_A} E \{ R_{ki} R_{kr} | \sigma_\Delta^2 \} Y_{li}^* Y_{rp} \Theta_{ilpr} \quad (39) \end{aligned}$$

$$\begin{aligned} E \left\{ \sum_{i=1}^{N_A} \eta_k^2 R_{ki}^2 \middle| \theta_k, \theta_d, \sigma_\Delta^2 \right\} \\ = E \{ \eta_k^2 \} \sum_{i=1}^{N_A} E \{ R_{ki}^2 | \sigma_\Delta^2 \} \quad (40) \end{aligned}$$

where  $\sigma_\Delta^2$  is the variance of the spatial AOA distribution  $f(\theta)$ .

Using (18)–(21), we express the cross-correlation matrix  $\mathcal{R}_{ij}$  between antenna elements  $i$  and  $j$  as

$$\mathcal{R}_{ij} = \begin{bmatrix} b_o & 0 & \rho_{R_i R_j} & \rho_{R_i I_j} \\ 0 & b_o & \rho_{I_i R_j} & \rho_{I_i I_j} \\ \rho_{R_i R_j} & -\rho_{I_i R_j} & b_o & 0 \\ \rho_{R_i I_j} & \rho_{I_i I_j} & 0 & b_o \end{bmatrix}. \quad (41)$$

In [33], it is shown that the cross-correlation between the Rayleigh distributed random variables at antennas  $i$  and  $j$  due

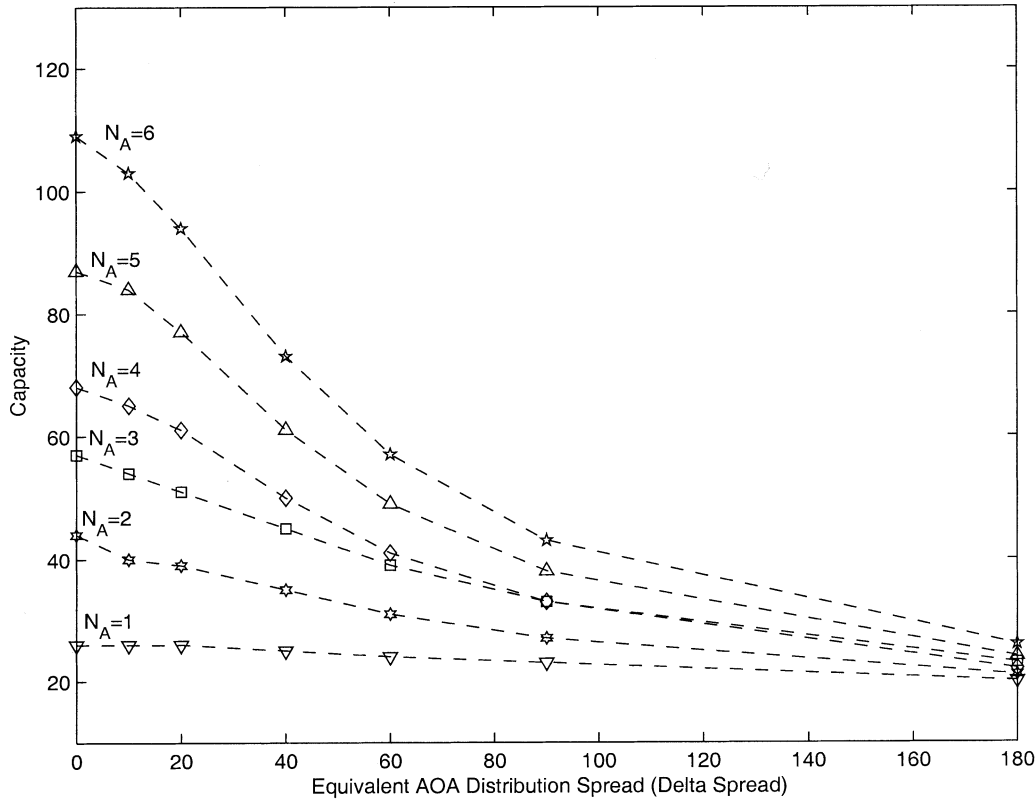


Fig. 5. System capacity predictions for a Gaussian angle-of-arrival distribution with mutual coupling.

to mobile  $k$  can be expressed in terms of the confluent hypergeometric function  ${}_2F_1(-1/2, -1/2; 1; \cdot)$  yielding

$$E\{R_{ki}R_{kj}\} = \frac{\pi}{2}b_o \left( {}_2F_1\left(-\frac{1}{2}, -\frac{1}{2}; 1; \zeta_{ji}^2\right) \right) \quad (42)$$

where

$$\zeta_{ji}^2 = \frac{\rho_{R_i R_j}^2 + \rho_{R_i I_j}^2}{b_o^2}. \quad (43)$$

Observing (22), (23), and (41), a decrease in correlation will occur as  $\sigma_{\Delta}^2$  increases, affecting the off-main diagonal matrix elements of  $\mathcal{R}_{ij}$ .

By substituting the above expressions, the normalized interference power (34) can be rewritten as

$$\begin{aligned} \phi_k(\theta_d, \theta_k) &= \left( 2N_A \sum_{h=1}^{N_A} \sum_{s=1}^{N_A} \sum_{m=1}^{N_A} e^{j(\alpha_h(\theta_d) - \alpha_s(\theta_d))} Y_{sm}^* Y_{mh} \right)^{-1} \quad (44) \\ &\cdot \frac{\pi}{2} b_o \sum_{i=1}^{N_A} \sum_{l=1}^{N_A} \sum_{p=1}^{N_A} \sum_{r=1}^{N_A} {}_2F_1\left(-\frac{1}{2}, -\frac{1}{2}; 1; \zeta_{ji}^2\right) Y_{li}^* Y_{rp} \Theta_{ilpr}. \quad (45) \end{aligned}$$

To compute  $E\{\tilde{P}_I\}$  in (29), (45) is averaged over a discretized set of angles  $\theta_k$  and  $\theta_d$ , i.e.,

$$E\{\tilde{P}_I\} = E\{\phi_k(\theta_d, \theta_k)\} = \frac{1}{N_{\theta}^2} \sum_{\theta_d \in \Theta_d} \sum_{\theta_k \in \Theta_k} \phi_k(\theta_k, \theta_d) \quad (46)$$

where  $\Theta_k$  and  $\Theta_d$  denote sets of  $N_{\theta}$  AOAs that range uniformly over  $[0, 2\pi)$  rad.

Similarly, the fraction of the desired signal being output by the beamformer for AOA  $\theta_d$  is given by

$$\tilde{P}_D(\theta_d) = \frac{2\pi}{N_{\theta}} \sum_{\theta \in \Theta} f(\theta) \phi_k(\theta, \theta_d) \quad (47)$$

where  $f(\theta)$  is the spatial azimuth distribution of the incoming signal,  $\Theta$  is a set of  $N_{\theta}$  AOAs that range uniformly over  $[0, 2\pi)$ , and  $\phi(\theta, \theta_d)$  is given by (45).

Finally, the expected power of the desired signal being output by the beamformer is

$$E\{\tilde{P}_D\} = E\{\tilde{P}_D(\theta_d)\} = \frac{2\pi}{N_{\theta}^2} \sum_{\theta_d \in \Theta_d} \sum_{\theta \in \Theta} f(\theta) \phi_k(\theta, \theta_d). \quad (48)$$

### B. Example: Gaussian Angle-of-Arrival Spatial Distribution

Suppose, for example, we use a Gaussian  $f(\theta)$  with mean  $\theta_d$  and variance equivalent to that of a uniform distribution over  $[\theta_d - \Delta, \theta_d + \Delta]$ . This yields

$$f(\theta) = \sqrt{\frac{3}{2\pi\Delta^2}} e^{-3(\theta - \theta_d)^2 / 2\Delta^2}. \quad (49)$$

In (49),  $\sigma_{\Delta}^2 = \Delta^2/3$ . Substituting (49) into (48) yields

$$E\{\tilde{P}_D\} = \frac{\sqrt{6\pi}}{N_{\theta}^2} \frac{1}{|\Delta|} \sum_{\theta_d \in \Theta_d} \sum_{\theta \in \Theta} e^{-3(\theta - \theta_d)^2/2\Delta^2} \phi_k(\theta, \theta_d) \quad (50)$$

where  $\Theta$  and  $\Theta_d$  are sets of  $N_{\theta}$  AOAs that range uniformly over  $[0, 2\pi)$ .

## V. IMPERFECT POWER-CONTROL EFFECTS

Perfect power control refers to the situation where the base-station receiver controls the transmission power of each mobile to a desired level precisely and instantaneously. A more realistic assumption, *imperfect power control*, also known as *slow* or *average* power control, refers to the situation where the base station is only able to control the longer term average transmission power levels, while ignoring fast Doppler fading amplitude fluctuations. In the following, we generalize the derivation of outage probability in [1] and [18] to the case of a base-station array with mutual coupling and scattering.

### A. Probability of Outage: Perfect Power Control

Assuming that we have a single cell occupied by  $k_u$  perfectly power-controlled users and an  $N_A$ -element base-station array with perfect power control, the total average power received by the cell assuming stationary arrivals is

$$\text{Total Power} = E\{\tilde{P}_D\}v_1 + \sum_{i=2}^{k_u} v_i E\{\tilde{P}_I\}E_b R_B + N_A N_o B \quad (51)$$

using terms defined in the previous section as well as user activity factor  $\alpha = \Pr\{v_i = 1\}$  and  $v_i$ , a binary random variable indicating user  $i$ 's activity. The desired mobile is denoted as  $i = 1$  without loss of generality.

From (51), we identify the average noise-plus-interference power as

$$I_o B = \sum_{i=2}^{k_u} v_i E\{\tilde{P}_I\}E_b R_B + N_A N_o B \quad (52)$$

where  $I_o$  is the noise-plus-interference power spectral density.

Due to dynamic range limitations, we limit the power ratio  $I_o B/N_o B$  such that

$$\frac{I_o}{N_o} < \frac{1}{\tau} \quad (53)$$

where  $\tau$  typically ranges between 0.25 and 0.1, i.e., 6–10 dB [1].

To obtain the probability of outage, we substitute (53) into (52), yielding the relationship

$$\sum_{i=2}^{k_u} v_i < \frac{I_o B (1 - \tau N_A)}{E\{\tilde{P}_I\}E_b R_B}. \quad (54)$$

The following tighter bound is used to reflect the fact that the bit energy-to-noise ratio for the desired user is also affected by beamforming:

$$\sum_{i=2}^{k_u} v_i < \frac{\left(\frac{B}{R_B}\right)(1 - \tau N_A)}{\frac{E\{\tilde{P}_I\}E_b}{E\{\tilde{P}_D\}I_o}} \equiv K'_o \quad (55)$$

where both  $v_i$  and  $k_u$  are independent random variables. Note that when (55) is not met, the system is said to be in *outage*. We also note that we are employing a stricter outage condition than in [1] and [18] by not including the  $v_1$  term in (55).

To simplify the notation, we define  $k'_u = k_u - 1$  to represent the number of interfering mobiles within the cell. Thus, the outage probability  $P_{\text{out}}$  is the probability that  $Z = \sum_{l=1}^{k'_u} v_l$  exceeds  $K'_o$ . Since we are assuming that the users remain in the system through outage, known as a *lost call hold* model,  $k'_u$  has a Poisson distribution with rate  $\alpha\lambda/\mu$ , where  $\lambda$  is the total average call arrival rate and  $\mu$  is the average call duration.

The moment-generating function of  $Z$  can be computed via

$$\begin{aligned} E\{e^{sZ}\} &= E_{k'_u} \prod_{l=1}^{k'_u} E_{v_l}(e^{sv_l}) \\ &= E_{k'_u} \prod_{l=1}^{k'_u} \left[ \Pr\{v_l = 1\} e^{s\{v_l=1\}} \right. \\ &\quad \left. + \Pr\{v_l = 0\} e^{s\{v_l=0\}} \right] \\ &= E_{k'_u} \prod_{l=1}^{k'_u} [\alpha e^s + (1 - \alpha)] \\ &= \sum_{k'_u=0}^{\infty} \frac{\left(\frac{\alpha\lambda}{\mu}\right)^{k'_u} [\alpha(e^s - 1) + 1]^{k'_u}}{k'_u!} e^{-\lambda/\mu} \\ &= \exp\left[\left(\frac{\alpha\lambda}{\mu}\right)(e^s - 1)\right]. \end{aligned} \quad (56)$$

Since (56) is the moment generating function of a Poisson distribution, the outage probability is just the sum of Poisson tails, namely

$$P_{\text{out}} = e^{-\alpha\lambda/\mu} \sum_{k=[K'_o]}^{\infty} \frac{\left(\frac{\alpha\lambda}{\mu}\right)^k}{k!}. \quad (57)$$

Alternatively,  $P_{\text{out}}$  may also be evaluated via its Chernoff bound

$$\begin{aligned} P_{\text{out}} &< \min_{s>0} \left\{ E\left\{e^{s(Z-K'_o)}\right\}\right\} \\ &= \min_{s>0} \left\{ e^{(\alpha\lambda/\mu)(e^s - 1)} e^{-sK'_o} \right\} \end{aligned}$$

where the minimum value of  $s$  is found as  $s = \ln(K'_o \mu / \alpha \lambda)$ . Therefore,  $P_{\text{out}}$  becomes

$$\begin{aligned} P_{\text{out}} &< \exp\left(\frac{\alpha \lambda}{\mu} e^{\ln(K'_o \mu / \alpha \lambda)} - \frac{\alpha \lambda}{\mu} - \ln\left(\frac{K'_o \mu}{\alpha \lambda}\right) K'_o\right) \\ &= \exp\left(-K'_o \left(\ln\left(\frac{K'_o}{\mu}\right) - 1 + \frac{\alpha \lambda}{K'_o}\right)\right). \end{aligned} \quad (58)$$

We can further approximate (58), for large  $K'_o$ , as a Gaussian variable with a mean and variance of  $\alpha \lambda / \mu$ , yielding

$$P_{\text{out}} \approx Q\left(\frac{K'_o - \frac{\alpha \lambda}{\mu}}{\sqrt{\frac{\alpha \lambda}{\mu}}}\right) \quad (59)$$

where  $Q(z) \equiv 1/2(1 - \text{erf}(z/\sqrt{2}))$ .

### B. Probability of Outage: Imperfect Power Control

Suppose now we loosen our restriction on perfect power control. A user that is controlled to a desired  $E_b/I_o$  level may now vary due to multipath propagation conditions according to a log-normal distribution with a standard deviation of about 1.5–2.5 dB [1], [18].

To account for the effects of imperfect power control, beamforming, scattering, and mutual coupling, we modify the derivation in the previous section as follows: instead of a constant  $E_b$ , let us define the bit energy to be  $\epsilon_l E_b$ , which is log-normally distributed. The outage probability under imperfect power control becomes

$$P_{\text{out,imp}} = \Pr\left\{Z' = \sum_{l=1}^{k'_u} \epsilon_l v_l > K'_o\right\}. \quad (60)$$

We define the following transformed random variable:

$$x_l = 10 \log_{10}\left(E\{\tilde{P}_I\} \epsilon_l \frac{E_b}{I_o}\right) \quad (61)$$

which is normally distributed with mean  $m_c$  and standard deviation  $\sigma_c$ . Exponentiating (61) yields

$$\frac{E_b}{I_o} \epsilon_l E\{\tilde{P}_I\} = 10^{x_l/10} = e^{\xi x_l} \quad (62)$$

where  $\xi = \ln(10)/10$ .

To solve for the moment-generating function of the random variable  $Z'$  in (60), we first evaluate

$$\begin{aligned} E\{\epsilon_l^n\} &= \left(\frac{E_b}{I_o} E\{\tilde{P}_I\}\right)^{-n} \int_{-\infty}^{\infty} e^{n \xi x_l} \frac{e^{-(x_l - m_c)^2 / (2\sigma_c^2)}}{\sqrt{2\pi\sigma_c^2}} dx_l \\ &= \frac{(e^{\xi m_c})^n}{\left(\frac{E_b}{I_o}\right)^n (E\{\tilde{P}_I\})^n} e^{n^2 (\xi \sigma_c)^2 / 2}. \end{aligned} \quad (63)$$

Redefining the arbitrary constant  $E_b$  in the above, we absorb the mean  $m_c$ , and (63) becomes

$$E\{\epsilon_l^n\} = e^{n^2 (\xi \sigma_c)^2 / 2}. \quad (64)$$

Since the moment-generating function of (64) is not finite, we resort to a modified Chernoff bound to obtain the outage probability [1]. This is accomplished by using a truncated moment-generating function approach, where the outage probability expression is broken up into two components. The first part is conditioned on  $v_l \epsilon_l < T$ , for all  $l$ , for some sufficiently large  $T$ , while the second part is conditioned on the complementary event. Therefore the probability of outage, upper bounding the second part of the expression by unity, becomes

$$\begin{aligned} P_{\text{out,imp}} &< \min_{s>0, T>0} \left\{ e^{\alpha(\lambda/\mu) E\{e^{s\epsilon_l} - 1\} - s K'_o} \right. \\ &\quad \left. + \alpha \left(\frac{\lambda}{\mu}\right) \Pr\{\epsilon \geq T\} \right\} \end{aligned} \quad (65)$$

where, by setting  $\xi = \ln(\epsilon)/\beta = x - m_c$ , knowing that  $\xi$  is Gaussian with zero mean and standard deviation  $\sigma_c$ , and defining  $\theta = \ln(T)/\beta$ , we have

$$\begin{aligned} E\{e^{s\epsilon_l}\} &= \frac{1}{\sqrt{2\pi\sigma_c^2}} \int_{-\infty}^{\theta} e^{s e^{\beta \xi}} e^{-\xi^2 / 2\sigma_c^2} d\xi \\ &= \sum_{n=0}^{\infty} \frac{s^n}{n!} e^{n^2 (\beta \sigma_c)^2 / 2} Q\left(n\beta\sigma_c - \frac{\theta}{\sigma_c}\right) \end{aligned} \quad (66)$$

and

$$\begin{aligned} \Pr\{\epsilon \geq T\} &= \frac{1}{\sqrt{2\pi}\sigma_c} \int_{\ln(T)/\beta}^{\infty} e^{-\xi^2 / 2\sigma_c^2} d\xi \\ &= Q\left(\frac{\theta}{\sigma_c}\right). \end{aligned} \quad (67)$$

As was described previously for the case of perfect power control, we can alternatively rewrite (60) in the form of a Gaussian approximation. Furthermore, it is no longer necessary to truncate the moments, since the untruncated first and second moments exist. Therefore, approximating the distribution of  $Z'$  in (60) yields

$$P_{\text{out,imp}} \approx Q\left(\frac{K'_o - \alpha \left(\frac{\lambda}{\mu}\right) e^{(\beta \sigma_c)^2 / 2}}{\sqrt{\alpha \left(\frac{\lambda}{\mu}\right) e^{2(\beta \sigma_c)^2}}}\right) \quad (68)$$

where we have used  $\sigma_c = 2.5$  dB.

## VI. CAPACITY RESULTS

We now compare the impact of the nonideal effects discussed in the previous sections on the uplink capacity of a single cell. Throughout, a Gaussian angle-of-arrival distribution of incoming plane waves is assumed.

The impact of mutual coupling on the system capacity from beamforming in a scattering environment as derived in (30) is depicted in Figs. 4 and 5. Clearly, these two effects deteriorate uplink CDMA system performance significantly. In partic-

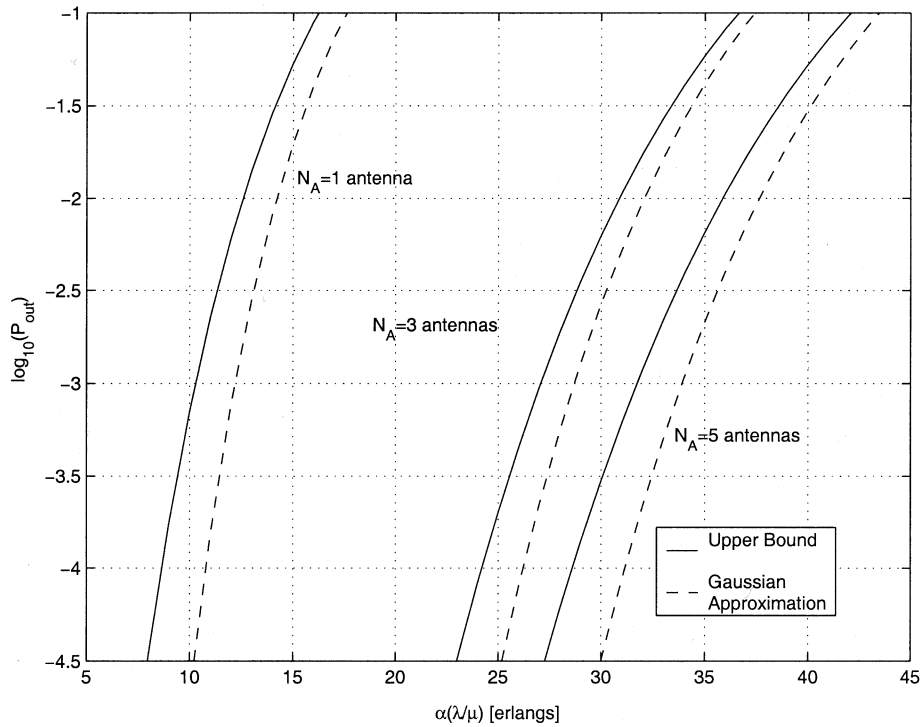


Fig. 6. Number of array elements versus outage probability with no mutual coupling, no scatter, and perfect power control.

ular, the performance degradation is dependent on the amount of angle spread present in the system. When the angle spread  $\Delta$  is less than approximately  $40^\circ$ , then mutual coupling degrades performance. For larger angle spreads, mutual coupling seems to improve performance slightly. As the angle spread approaches  $180^\circ$ , the beamforming gain diminishes to that of a single antenna, as expected, since the scatter is completely enveloping the array, nullifying any capacity advantage of digital beamforming.

Using (57), (59), (65), and (68), the joint impact of mutual coupling, scattering, and power control on system performance are examined in the remaining figures, which depict the log-probability of outage versus normalized average user occupancy in erlangs. Occupancy consists of the rate term  $\alpha(\lambda/\mu)$ , where  $\lambda$  is the total mean call arrival rate,  $\mu$  is the mean service time, and  $\alpha$  is the activity factor.

Fig. 6 exhibits performance as a function of the number of array elements with perfect power control, no mutual coupling, and no scattering. Equations (57) and (59) are plotted for a one-, three-, and five-element base-station antenna array, showing improvement in outage probability as the number of antennas increases. Fig. 7, generated using (65) and (68), shows the performance loss due to imperfect power control.

Fig. 8 exhibits the effects of mutual coupling and scattering under perfect power control for a five-element antenna array. Figs. 9 and 10 show imperfect power-control effects. Two values of angle spread are used:  $\Delta = 15^\circ$ , corresponding to hilly terrain in a macrocell (Fig. 9), and  $\Delta = 60^\circ$ , corresponding to a microcell [22] (in a mall) (Fig. 10). With mutual coupling and  $\Delta = 60^\circ$ , we achieve the lowest performance of the four cases, followed by mutual coupling and  $\Delta = 15^\circ$  and, finally, mutual coupling and no scatter.

We have also repeated the above comparisons on three-element circular arrays and obtained similar results, but have omitted these figures due to space considerations. At an angle spread of  $15^\circ$ , with mutual coupling effects, and operating under imperfect power control (Gaussian approximation) conditions, increasing the array from three to five elements resulted in a system utilization increase from 18 to 22 erlangs at a probability of outage of  $10^{-3}$ , while at a  $60^\circ$  angle spread, there was no significant difference in utilization. We therefore conclude that capacity gains due to beamforming are still possible despite these nonideal effects.

## VII. CONCLUSIONS

The induced EMF method [6], the method of moments [7], and full-wave electromagnetic numerical computation [21] were used to model the effects of mutual coupling on beam-pattern synthesis and were then applied to uplink CDMA system capacity prediction. Mutual coupling creates beam patterns with higher sidelobe levels, shallower nulls, and wider beamwidths. We observed that for the case of circular arrays, the beam patterns for all three methods compare closely to one another. We have quantified uplink CDMA system performance in the presence of mutual coupling. We observe a capacity reduction of 6–11% for the case of a five-element circular array due to mutual coupling.

We then considered the combined effects of mutual coupling and scattering (angle spread) due to multipath by determining the cross-correlation statistics between antennas of the array. At large angle spread, scattering is a dominant degradation factor. An angle spread of  $\Delta = 10^\circ$  yields a capacity decrease of 10–14.5% due to mutual coupling. At the other extreme, if the

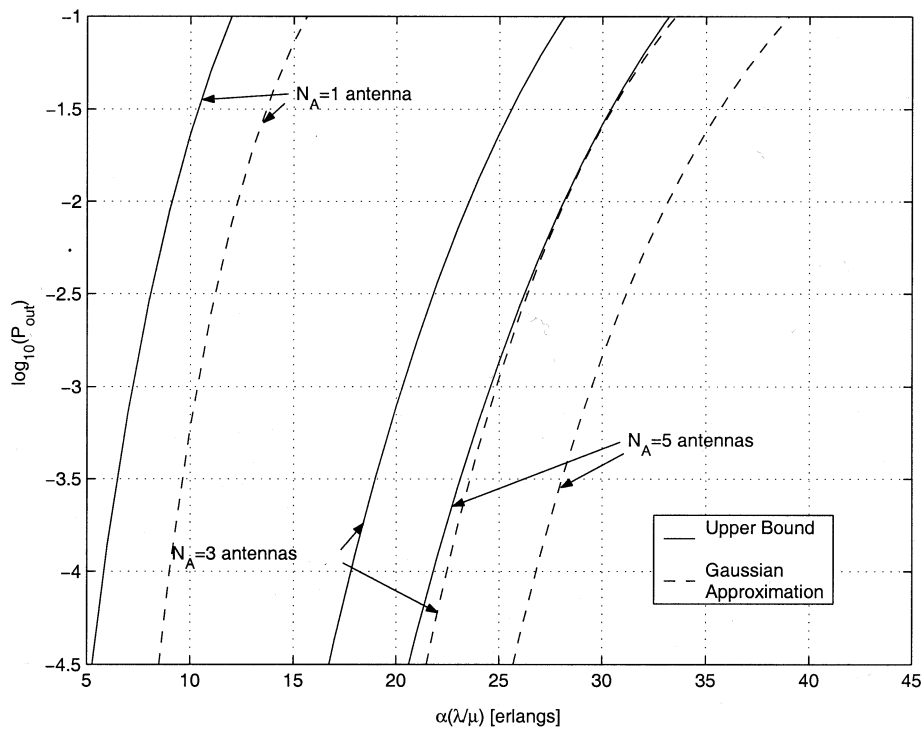


Fig. 7. Number of array elements versus outage probability with no mutual coupling, no scatter, and imperfect power control.

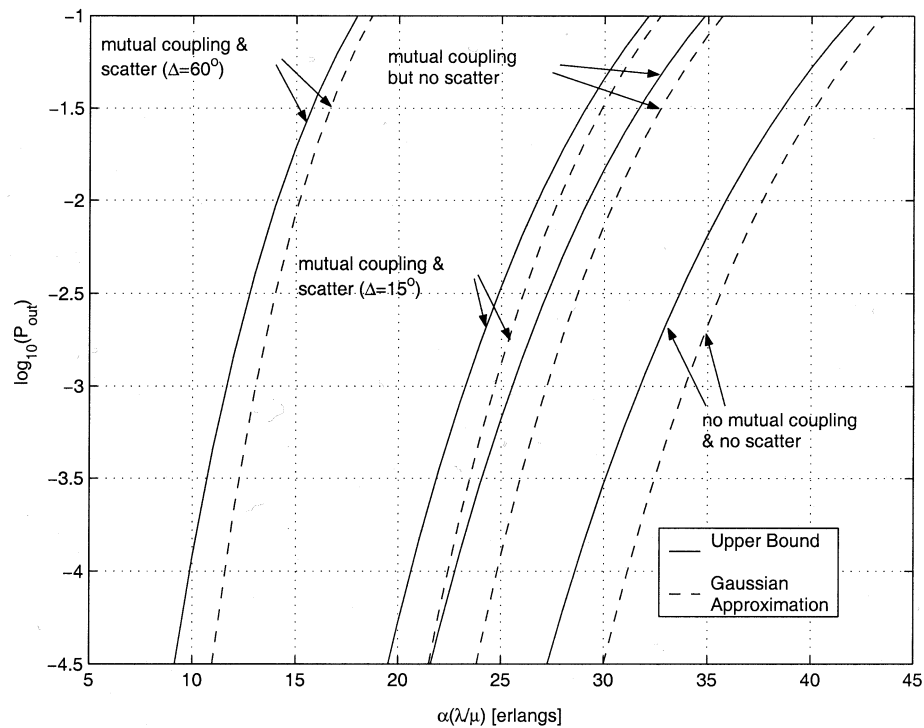


Fig. 8. Effect of mutual coupling and scatter on outage probability with five antennas and perfect power control.

angle spread approaches  $\Delta = 180^\circ$ , system capacity decreases to that of a single antenna.

The combination of imperfect power control was then added. The probability of outage was derived based on extending [1] and [18] to multiple antennas, mutual coupling, and scattering. Expressions were developed for outage probability under perfect and

imperfect power control, including an upper bound and a Gaussian approximation. As expected, imperfect power control causes additional degradation. Despite these nonideal effects, increasing the number of antennas was shown to improve uplink capacity.

Although more detailed than previous work, simplifications were employed nevertheless: first, the capacity results only

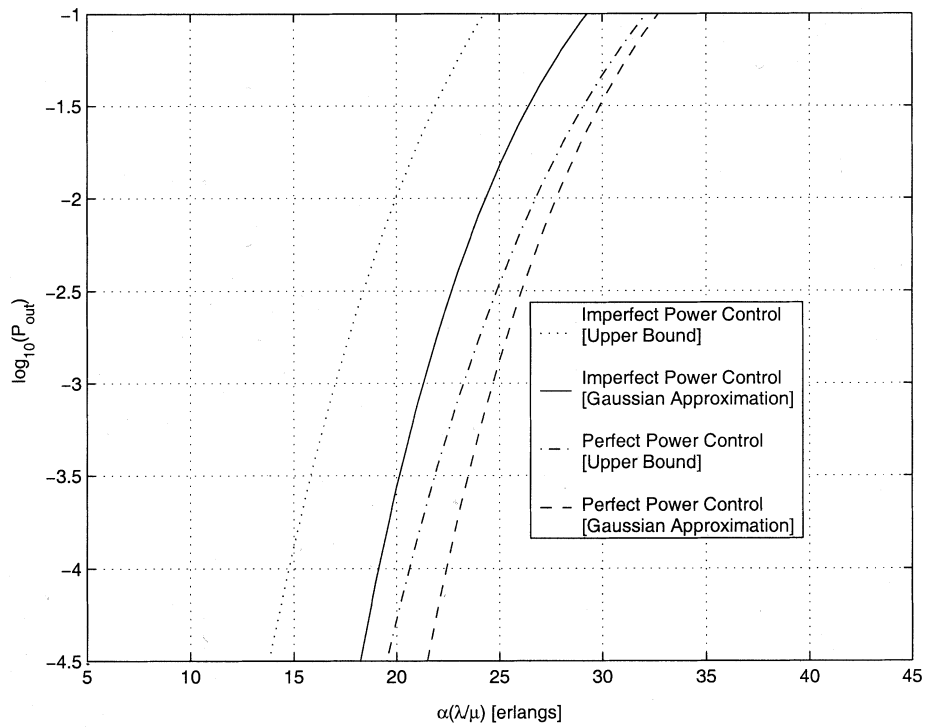


Fig. 9. Effect of imperfect power control on outage probability, five antennas, mutual coupling, and  $\Delta = 15^\circ$ .

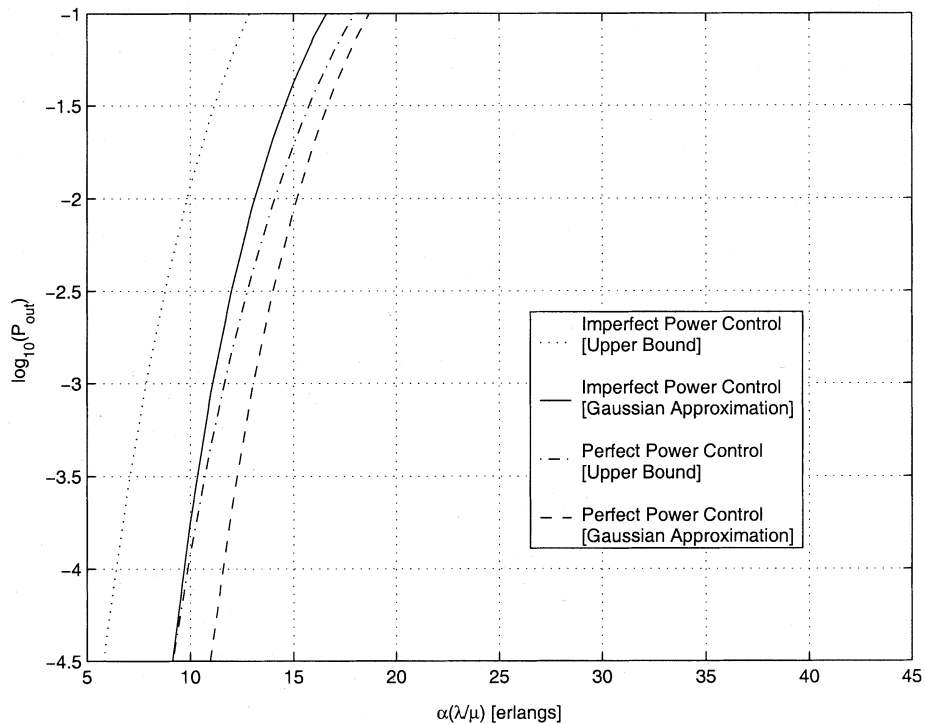


Fig. 10. Effect of imperfect power control on outage probability, five antennas, mutual coupling, and  $\Delta = 60^\circ$ .

consider a single cell and are therefore optimistic. Second, resolvable multipath delay spread as encountered in wide-band CDMA has not been considered. While the diversity of a resolvable multipath may, in principle, be exploited, this would be offset by an overall increase in multiple-access interference. Finally, it should be noted that multiple transmit antennas may

be used for channels with high angle spread to realize much larger capacity gains than reported here.

#### APPENDIX

In the following, we derive the second moment  $\overline{B_{ic}B_{ic}^*}$ . The other second moments follow in a similar manner. Starting with

(12), (13), and (17)

$$\begin{aligned}
& \overline{B_{ic} B_{ic}^*} \\
&= E \left\{ \left( |Y_{ii}| A_i \cos(\Psi_1) e^{j\angle Y_{ii}} + |Y_{ik}| A_k \cos(\Psi_2) e^{j\angle Y_{ik}} \right) \right. \\
& \quad \cdot \left. \left( |Y_{ii}| A_i \cos(\Psi_1) e^{j\angle Y_{ii}} + |Y_{ik}| A_k \cos(\Psi_2) e^{j\angle Y_{ik}} \right)^* \right\} \\
&= E \left\{ \left( |Y_{ii}| A_i \cos(\Psi_1) e^{j\angle Y_{ii}} + |Y_{ik}| A_k \cos(\Psi_2) e^{j\angle Y_{ik}} \right) \right. \\
& \quad \cdot \left. \left( |Y_{ii}| A_i \cos(\Psi_1) e^{-j\angle Y_{ii}} + |Y_{ik}| A_k \cos(\Psi_2) e^{-j\angle Y_{ik}} \right) \right\} \\
&= E \left\{ |Y_{ii}|^2 A_i^2 \cos^2(\Psi_1) + |Y_{ik}|^2 A_k^2 \cos^2(\Psi_2) \right. \\
& \quad + |Y_{ii}| |Y_{ik}| A_i A_k \cos(\Psi_1) \cos(\Psi_2) e^{j(\angle Y_{ii} - \angle Y_{ik})} \\
& \quad \left. + |Y_{ii}| |Y_{ik}| A_i A_k \cos(\Psi_1) \cos(\Psi_2) e^{j(\angle Y_{ik} - \angle Y_{ii})} \right\} \\
&= E \left\{ |Y_{ii}|^2 A_i^2 \left( \frac{1}{2} + \frac{1}{2} \cos(2\Psi_1) \right) \right. \\
& \quad + |Y_{ik}|^2 A_k^2 \left( \frac{1}{2} + \frac{1}{2} \cos(2\Psi_2) \right) \\
& \quad \left. + 2 |Y_{ii}| |Y_{ik}| A_i A_k \cos(\Psi_1) \cos(\Psi_2) \cos(\angle Y_{ii} - \angle Y_{ik}) \right\} \\
&= E \left\{ |Y_{ii}|^2 A_i^2 \left( \frac{1}{2} + \frac{1}{2} \cos(2\Psi_1) \right) \right. \\
& \quad + |Y_{ik}|^2 A_k^2 \left( \frac{1}{2} + \frac{1}{2} \cos(2\Psi_2) \right) \\
& \quad + |Y_{ii}| |Y_{ik}| A_i A_k (\cos(\Psi_1 + \Psi_2) \\
& \quad \left. + \cos(\Psi_1 - \Psi_2)) \cos(\angle Y_{ii} - \angle Y_{ik}) \right\} \\
&= \frac{1}{2} |Y_{ii}|^2 \overline{A_i^2} + \frac{1}{2} |Y_{ik}|^2 \overline{A_k^2} \\
& \quad + |Y_{ii}| |Y_{ik}| \overline{A_i A_k} \cos(\Psi_1 - \Psi_2) \cos(\angle Y_{ii} - \angle Y_{ik}) \\
&= \left( |Y_{ii}|^2 + |Y_{ik}|^2 \right) \frac{1}{2} \sum_{r=1}^m a_r^2 |Y_{ii}| |Y_{ik}| \\
& \quad + \sum_{r=1}^m a_r^2 \cos\left(\frac{2\pi d}{\lambda} \cos(\theta_{kr})\right) \cos(\angle Y_{ii} - \angle Y_{ik}) \quad (69)
\end{aligned}$$

which agrees with (18).

#### ACKNOWLEDGMENT

The authors would like to thank the anonymous reviewers for their careful reading of this paper as well as their suggestions and comments.

#### REFERENCES

- [1] A. J. Viterbi, *CDMA: Principles of Spread Spectrum Communication*. Reading, MA: Addison-Wesley, 1995.
- [2] A. F. Naguib and A. Paulraj, "Performance of wireless CDMA with M-ary orthogonal modulation and cell site antenna arrays," *IEEE J. Select. Areas Commun.*, vol. 14, no. 9, pp. 1770–1783, 1996.
- [3] A. M. Earnshaw and S. D. Blostein, "Efficient evaluation of adaptive digital beamforming for multi-service provision in a cellular CDMA system," *Proc. IEEE VTS 48th Veh. Technol. Conf.*, vol. 3, pp. 1665–1669, 1998.
- [4] P. J. McLane and S. Subramanian, "Erlang capacity of CDMA systems with adaptive arrays," in *Proc. VTC2000-Fall*, 2000.
- [5] P. S. Carter, "Circuit relations in radiating systems and applications to antenna problems," in *Proc. IRE*, vol. 20, June 1932, pp. 1004–1041.
- [6] H. E. King, "Mutual impedance of unequal length antennas in echelon," *IRE Trans. Antennas Propagat.*, vol. 5, pp. 306–313, July 1957.

- [7] R. F. Harrington, *Field Computation by Moment Method*. New York: MacMillan, 1968.
- [8] B. T. Strait and A. T. Adams, "Analysis and design of wire antennas with applications to emc," *IEEE Trans. Electromagn. Compat.*, vol. 12, no. EC-2, pp. 45–54, May 1970.
- [9] R. S. Adve and T. K. Sarkar, "Compensation for the effects of mutual coupling on direct data domain adaptive algorithms," *IEEE Trans. Antennas Propagat.*, vol. 48, pp. 86–94, Jan. 2000.
- [10] J. D. Krauss, *Antennas*, 2nd ed. New York: McGraw-Hill, 1988.
- [11] J. F. Diouris, S. McLaughlin, and J. Zeidler, "Sensitivity analysis of the performance of a diversity receiver," in *Proc. IEEE ICC*, 1999, pp. 1–5.
- [12] J. Luo, J. Zeidler, and S. McLaughlin, "Sensitivity analysis of compact antenna arrays in correlated Nakagami fading channels," *Proc. IEEE VTC Fall*, pp. 3.8.1.18.1–3.8.1.18.6, 2000.
- [13] —, "Performance analysis of compact antenna arrays with MRC in correlated Nakagami fading," *IEEE Trans. Veh. Technol.*, vol. 50, pp. 267–277, Jan. 2001.
- [14] G. W. K. Colman, "An investigation into the capacity of cellular CDMA communications systems with beamforming in environments with scatter," M.S. thesis, Queen's Univ., Canada, 1998.
- [15] E. N. Bramley, "Diversity effects in spaced-aerial reception of ionospheric waves," *Proc. Inst. Elect. Eng.*, vol. 98, no. 3, pp. 19–25, 1951.
- [16] W. C. Jakes, *Mobile Microwave Communications*. New York: Wiley, 1974.
- [17] J. Salz and J. H. Winters, "Effect of fading correlation on adaptive arrays in digital mobile radio," *IEEE Trans. Veh. Technol.*, vol. 43, pp. 1049–1057, Nov. 1994.
- [18] A. M. Viterbi and A. J. Viterbi, "Erlang capacity of a power controlled CDMA system," *IEEE J. Select. Areas Commun.*, vol. 11, no. 6, pp. 892–900, 1993.
- [19] T. Svantesson and A. Ranheim, "Mutual coupling effects on the capacity of multielement antenna systems," in *Proc. IEEE ICASSP*, vol. 4, 2001, pp. 2485–2488.
- [20] A. M. Wyglinski and S. D. Blostein, "Antenna array mutual coupling effects on cellular CDMA communication systems," in *Proc. 20th Biennial Symp. Commun.*, 2000, pp. 181–185.
- [21] Zeland, *IE3D Electromagnetic Simulator: User Manual*, 5th ed: Zeland Software, 1999.
- [22] A. F. Naguib, "Adaptive antennas for CDMA wireless networks," Ph.D. dissertation, Stanford Univ., 1995.
- [23] J. C. Liberti Jr and T. S. Rappaport, *Smart Antennas for Wireless Communications: IS95 and Third Generation CDMA Applications*. Englewood Cliffs, NJ: Prentice-Hall, 1999.
- [24] R. B. Ertel, P. Cardieri, K. W. Sowerby, T. S. Rappaport, and J. H. Reed, "Overview of spatial channel models for antenna array communication systems," *IEEE Personal Commun.*, vol. 5, pp. 10–22, Feb. 1998.
- [25] A. Moustakas, I. Corden, and A. Kogiantis, "Parameter mapping for spatial channel modeling," 3GPP2-C50–20010709, 2001.
- [26] A. Moustakas, M. Buehrer, and I. Corden, "Spatial channel model for the evaluation of MIMO architectures," 3GPP2-C50–20010611, 2001.
- [27] R. M. Buehrer, S. Arunachalam, K. Wu, and A. Tonello, "Spatial channel model and measurements for IMT-2000 systems," *Proc. IEEE VTC*, May 2001.
- [28] K. I. Pedersen, P. E. Mogensen, and B. H. Fleury, "A stochastic model of the temporal and azimuthal dispersion seen at the base station in outdoor propagation environments," *IEEE Trans. Veh. Technol.*, vol. 49, pp. 437–447, Mar. 2000.
- [29] K. S. Gilhousen, I. M. Jacobs, R. Padovani, A. J. Viterbi, L. A. Weaver, and C. E. Wheatley III, "On the capacity of a cellular CDMA system," *IEEE Trans. Veh. Technol.*, vol. 40, pp. 303–312, May 1991.
- [30] A. M. Wyglinski and S. D. Blostein, "Mutual coupling and scattering effects on cellular CDMA systems using smart antennas," in *Proc. IEEE VTC Fall*, 2000, pp. 3.8.1.12.1–3.8.1.12.6.
- [31] A. M. Wyglinski, "Performance of CDMA systems using digital beamforming with mutual coupling and scattering effects," M.S. thesis, Queen's Univ., Canada, 2000.
- [32] J. E. Hudson, *Adaptive Array Principles*. Stevenage, U.K.: Peregrinus, 1981.
- [33] W. B. Davenport Jr and W. L. Root, *An Intro to the Theory of Random Signals and Noise*. New York: McGraw-Hill, 1994.
- [34] A. Papoulis, *Probability, Random Variables, and Stochastic Processes*, 3rd ed. New York: McGraw-Hill, 1991.
- [35] W. C.-Y. Lee, "Effects on correlation between two mobile radio base-station antennas," *IEEE Trans. Commun.*, vol. COM-21, pp. 1214–1224, Nov. 1973.



**Alexander M. Wyglinski** (S'99) was born in Montréal, PQ, Canada, in 1975. He received the B.Eng. degree (with distinction) from McGill University, Montréal, in 1999 and the M.Sc.(Eng.) degree from Queen's University, Kingston, ON, Canada, in 2000, both in electrical engineering. He is currently pursuing the Ph.D. degree in electrical engineering at McGill University.

He was with the Department of National Defence, Ottawa, ON, Canada, as a Defence Research Assistant during the summers of 1997 and 1998. His current research interests lie in multirate signal processing, array signal processing, wireless communications, and data transmission.

Mr. Wyglinski received the Le Fonds FCAR scholarship from the Government of Québec and two consecutive Queen's Graduate Awards. He holds an NSERC Postgraduate Scholarship.



**Steven D. Blostein** (S'83–M'88–SM'96) received the B.S. degree in electrical engineering from Cornell University, Ithaca, NY, in 1983 and the M.S. and Ph.D. degrees in electrical and computer engineering from the University of Illinois, Urbana-Champaign, in 1985 and 1988, respectively.

He has been on the Faculty of Queen's University, Kingston, ON, Canada, since 1988 and currently is a Professor in the Department of Electrical and Computer Engineering. He has been a Consultant to both industry and government in the areas of document image compression, motion estimation, and target tracking. He was a Visiting Associate Professor in the Department of Electrical Engineering, McGill University, Canada, in 1995. His current interests lie in statistical signal processing, wireless communications, and video image communications. He currently leads the Multirate Wireless Data Access Major Project sponsored by the Canadian Institute for Telecommunications Research.

Prof. Blostein was Chair of the IEEE Kingston Section in 1993–1994, and Associate Editor of the IEEE TRANSACTIONS ON IMAGE PROCESSING in 1996–2000. He is a registered Professional Engineer in Ontario.